Laser-induced breakdown spectroscopy of copper with a 2 μm thulium fiber laser

Matthieu Baudelet,* Christina C. C. Willis, Lawrence Shah, and Martin Richardson

Townes Laser Institute, CREOL — The College of Optics and Photonics, University of Central Florida, Orlando, FL 32816, USA

** baudelet@creol.ucf.edu*

Abstract: We report the first implementation of a 2 μm thulium fiber laser in a Laser-Induced Breakdown Spectroscopy system. Emission from plasma on copper samples was analyzed from 200 to 900 nm. The low ablation fluence (<100 J.cm^{-2}) and 200 ns pulse duration lead to a plasma with neither continuum emission, nor air emission in the near-infrared region.

©2010 Optical Society of America

OCIS codes: (060.3510) Lasers, fiber; (300.6365) Spectroscopy, laser induced breakdown; (350.5400) Plasmas.

References and links

1. J. Debras-Guédon, and N. Liodec, "De l'utilisation du faisceau d'un amplificateur a ondes lumineuses par émission induite de rayonnement (laser à rubis), comme source énergétique pour l'excitation des spectres d'émission des éléments," C. R. Acad. Sci. **257**, 3336 (1963).
2. B. N. Chichkov, C. Momma, S. Nolte, F. von Alvensleben, and A. Tünnermann, "Femtosecond, picosecond and nanosecond laser ablation of solids," Appl. Phys., A Mater. Sci. Process. **63**(2), 109–115 (1996).
3. M. Baudelet, L. Guyon, J. Yu, J.-P. Wolf, T. Amodeo, E. Frejafon, and P. Laloi, "Femtosecond time-resolved laser-induced breakdown spectroscopy for detection and identification of bacteria: A comparison to the nanosecond regime," J. Appl. Phys. **99**(8), 084701 (2006).
4. Y. Kawamura, K. Toyoda, and S. Namba, "Effective deep ultraviolet photoetching of polymethyl methacrylate by an excimer laser," Appl. Phys. Lett. **40**(5), 374 (1982).
5. A. Khachatrian, and P. J. Dagdigian, "Laser-induced breakdown spectroscopy with laser irradiation on mid-infrared hybride stretch transitions: polystyrene," Appl. Phys. B **97**(1), 243–248 (2009).
6. A. W. Miziolek, V. Palleschi, and I. Schechter, *Laser-Induced Breakdown Spectroscopy (LIBS) – Fundamentals and Applications* (Cambridge University Press, 2006).
7. D. A. Cremers, and L. J. Radziemski, *Handbook of Laser-Induced Breakdown Spectroscopy* (John Wiley & Sons, 2006)
8. J. P. Singh, and S. N. Thakur, *Laser-Induced Breakdown Spectroscopy* (Elsevier Science Publishing, 2007)
9. D. E. Chung, and A. E. Te, "New techniques for laser prostatectomy: an update," Ther. Adv. Urol. **1**(2), 85–97 (2009).
10. J. A. Curcio, and C. C. Petty, "The Near Infrared Absorption Spectrum of Liquid Water," J. Opt. Soc. Am. **41**(5), 302–304 (1951).
11. M. von Allmen, and A. Blatter, *Laser-Beam Interactions with Materials – Physical Principles and Applications* (Springer, 1995)
12. M. Baudelet, L. Shah, C. Willis, and M. Richardson, "Laser-induced Breakdown Spectroscopy of Organic Materials with a Mid-IR Thulium-fiber-laer Nanosecond Pulse at 2μm" presented at the 2nd North America Symposium on Laser-Induced Breakdown Spectroscopy, New Orleans, LA, USA, 13–15 July 2009.
13. M. Sabsabi, F. R. Doucet, P.-P. Berube, and P. Bouchard, "Use of high-power pulsed fiber lasers for LIBS analysis: is it a useful tool?" presented at the 2nd North America Symposium on Laser Induced Breakdown Spectroscopy, New Orleans, LA, USA, 13–15 July 2009.
14. C. C. C. Willis, L. Shah, M. Baudelet, T. S. McComb, R. A. Sims, V. Sudesh, and M. C. Richardson, "High-energy Q-switched Tm^{3+}-doped polarization maintaining silica fiber laser", paper 7580–2 to be published in Photonics West 2010, *Proc. SPIE* **7580** (2010).
15. A. W. Snyder, and J. D. Love, *Optical Waveguide Theory* (Chapman & Hall, New York, 1983).
16. G. P. Agrawal, Nonlinear Fiber Optics, 4th ed. (2007)
17. F. Di Teodoro, and C. D. Brooks, "Multi-mJ Energy, Multi-MW Peak-Power Photonic Crystal Fiber Amplifiers with Near-Diffraction-Limited Output," in *Conference on Lasers and Electro-Optics/Quantum Electronics and Laser Science Conference and Photonic Applications Systems Technologies*, OSA Technical Digest Series (CD), Optical Society of America, Washington DC 2007, paper CFI3.
18. G. W. Rieger, M. Taschuk, Y. Y. Tsui, and R. Fedosejevs, "Comparative study of laser-induced plasma emission from microjoule picosecond and nanosecond KrF-laser pulses," Spectrochim. Acta, B At. Spectrosc. **58**(3), 497–510 (2003).

#123146 - $15.00 USD Received 21 Jan 2010; revised 27 Mar 2010; accepted 29 Mar 2010; published 31 Mar 2010
(C) 2010 OSA

19. Y. Ralchenko, A.E. Kramida, J. Reader and NIST ASD Team (2008). *NIST Atomic Spectra Database* (version 3.1.5), [Online]. Available: http://physics.nist.gov/asd3 [2009, October 1]. National Institute of Standards and Technology, Gaithersburg, MD.
20. A. G. Shenstone, "The first spectrum of copper (Cu I)," Philos. Trans. R. Soc. Lond. A **241**(832), 297–322 (1948).
21. A. Kono, and S. Hattori, "Lifetimes and transition probabilities in Cu II," J. Opt. Soc. Am. **72**(5), 601–605 (1982).
22. G. Cristoforetti, A. De Giacomo, M. Dell'Aglio, S. Legnaioli, E. Tognoni, V. Palleschi, and N. Omenetto, "Local Thermodynamic Equilibrium in laser-Induced Breakdown Spectroscopy: Beyond the McWhirter Criterion," Spectrochim. Acta, B At. Spectrosc. **65**(1), 86–95 (2010).
23. M. Baudelet, M. Boueri, J. Yu, S. S. Mao, V. Piscitelli, X. Mao, and R. E. Russo, "Time-resolved ultraviolet laser-induced breakdown spectroscopy for organic material analysis," Spectrochim. Acta, B At. Spectrosc. **62**(12), 1329–1334 (2007).

1. Introduction

Laser-Induced Breakdown Spectroscopy (LIBS) has continued to develop since its first analytical application in 1963 [1]. The evolution of the laser has allowed LIBS techniques to expand into new regimes of ablation, which have improved results and expanded the range of targets that can be characterized. For instance, femtosecond lasers have revolutionized the quantitation of the ablated mass thanks to a cleaner ablation [2] and allow a better detection of trace elements thanks a low continuum emission from the induced plasmas [3]; polymer ablation and analysis has been improved by the introduction of the ultraviolet lasers [4] and mid-infrared pulses generated from optical parametric amplification [5] making the ablation resonant with absorption bands. Lasers currently used in LIBS are predominantly solid-state lasers (Nd:YAG, Ti:Sapphire), gas lasers (CO_2), and excimer lasers (KrF) [6–8]; however excitation and ablation has expanded to the 2 μm regime with the introduction of holmium and thulium based lasers. Their use in medical laser ablation [9] has become of great interest due to the fact that their emission around 2 μm overlaps several water absorption peaks [10]. Q-switching these lasers can generate nanosecond pulses, providing focused irradiances within the necessary range for plasma generation ($GW.cm^{-2}$) [11]. Fiber lasers have rarely been used as sources for LIBS [6,12,13], but they have several distinct advantages over other sources including compactness, simplified thermal management, overall high efficiency and near-diffraction limited beam quality even at high average power.

In this study we report the use of a thulium fiber laser for LIBS of a copper sample. Although the technology has not yet matured, Tm:fiber lasers with wavelengths around 2 μm offer great potential for high peak power scaling due to significantly lower nonlinearities than for standard fiber laser operating at 1 and 1.5 μm. We believe the output pulse energy of nanosecond thulium fiber laser systems can be increased well beyond the milliJoule level, making such systems appropriate for a wide variety of ablation applications. As an exploratory effort, we characterize the emission spectrum generated by irradiation with ~200 ns pulse at 2 μm wavelength in order to evaluate the analytical advantages and consider the potential of Tm:fiber lasers for LIBS applications.

2. Experimental setup

Our experimental setup (Fig. 1) consisted of a Q-switched Tm:fiber laser, a motorized translation stage for sample positioning, and a time-resolved detection setup composed of an Echelle spectrometer with an iCCD camera.

2.1 Laser source

The laser source (dotted box in Fig. 1) was an actively Q-switched Tm^{3+}-doped, polarization maintaining, silica, large mode area fiber laser. A detailed description of the laser

#123146 - $15.00 USD Received 21 Jan 2010; revised 27 Mar 2010; accepted 29 Mar 2010; published 31 Mar 2010
(C) 2010 OSA

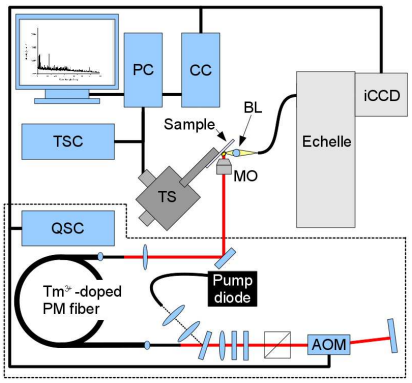

Fig. 1. Experimental setup. AOM: Acousto-optic modulator, QSC:Q-Switch controller, MO: Microscope objective, TS: translation stage, TSC: motion controller, BL: ball lens, iCCD: intensified CCD, CC: camera controller, PC: computer.

may be found in Willis *et al.* [14]. The laser delivered pulse energies of 100 µJ to the target with 200 ns pulse duration at 1992 nm with a repetition rate of 20 kHz.

Although the laser system does not outperform its 1 and 1.55 µm counterparts in terms of power, it does possess several advantages unique to its 2 µm wavelength operation. These advantages should make it possible to increase the pulse energy to be competitive with conventional solid-state lasers. For example, the V parameter, which defines the single-mode propagation cut-off, is proportional to the fiber core diameter divided by the laser wavelength [15]. Therefore, the longer operational wavelength of Tm:fiber makes it possible to utilize mode field areas 4 (MA 2.6) times larger than for 1 (MA 1.5) µm wavelengths without sacrificing mode quality. In addition to enabling the use of fibers with larger mode area, the critical powers for stimulated Raman scattering, stimulated Brillouin scattering, and self-focusing increase with laser wavelength [16]. As such, Tm:fiber lasers have the potential to allow peak power scaling beyond the MW-level limit that is associated with nanosecond pulses in ytterbium fiber laser systems [17].

2.2 Sample holder

The focal waist diameter of the beam was ~10 µm at an angle of 45° to the normal of the sample. It was focused using an 11 mm focal length, 0.3 NA (full aperture) asphere microscope objective providing ~95% transmission at 2 µm. The irradiance on the target was 600 $MW.cm^{-2}$. The sample was positioned using three motorized translation stages (VP-25XA with an ESP300 motion controller, Newport) in an X-Y-Z configuration allowing a displacement of the sample at a speed of 25 mm/s.

2.3 Detection

The plasma emission was collected by an f/2 UV-transmissive collimating ball-lens (74-UV, Ocean Optics) which coupled light into a 1-meter UV transmissive 200-µm-core fiber (HRE-FBR-1M, Princeton Instruments). This fiber was coupled to a 250 mm Echelle spectrometer (Acton HRE, Princeton Instruments) combined with a 1024x1024 pixels GenII iCCD camera with a MgF_2 input window and a P46 phosphor (PI-MAX2, Princeton Instruments). This configuration gave a resolution of 0.04 nm from 200 to 900 nm.

The system was spectrally calibrated with a mercury lamp (PenRay, UVP) and the spectral response of the system was calibrated with two calibrated radiometric sources: a deuterium lamp (Model 63979, Newport) for the 200-400 nm spectral range and a quartz-tungsten lamp (QTH, Newport) for the 400-900 m spectral range.

Each time-integrated spectrum consisted of 5000 single-shot spectra, as the result of 5 accumulations of 1000 gated detections per CCD exposure time (50 ms). Each single-shot detection began 100 ns before the laser pulse and had a 400 ns duration. Because of the short

#123146 - $15.00 USD Received 21 Jan 2010; revised 27 Mar 2010; accepted 29 Mar 2010; published 31 Mar 2010
(C) 2010 OSA

lifetime of the plasma, it was not possible to obtain time-resolved spectra with a reasonable signal-to-noise ratio. In order to provide statistics on the temperature measurements, 30 spectra were taken successively.

2.4 Samples

The samples studied were cut from a 0.25 mm-thick foil of 99.98% copper (349178, Sigma-Aldrich). Each sample was cleaned with acetone before every ablation run in order to remove any oxidation layers.

3. Results and discussion

The spectra taken from the copper spanned from 200 nm to 900 nm. Emission transitions were all from neutral and singly-ionized copper and are shown in Fig. 2. The sawtooth-like background in the spectrum is due to the correction of the spectral sensitivity of the acquisition system showing the different orders of the Echelle spectrometer. The declining background in the ultraviolet region is the consequence of this spectral response correction and the low efficiency of the system in this spectral region.

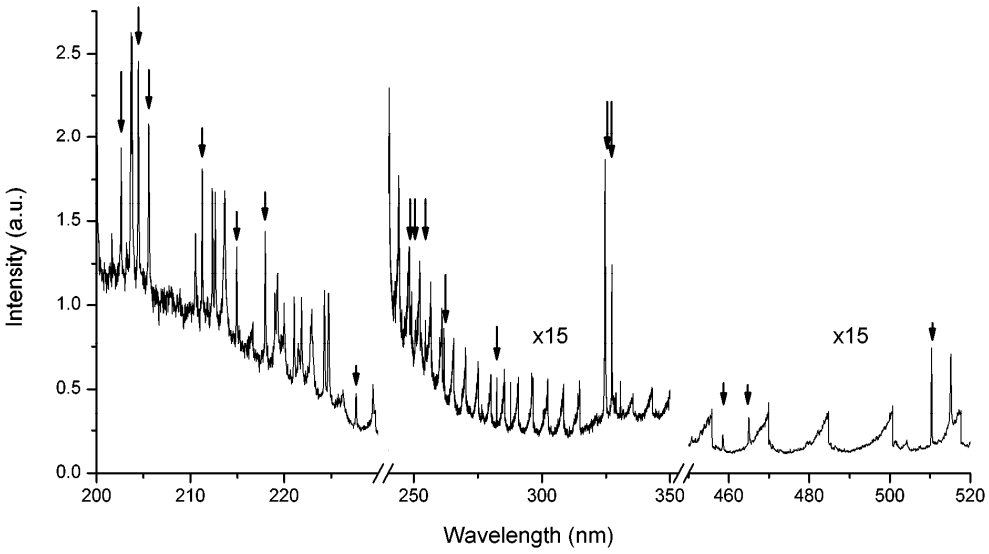

Fig. 2. Spectrum from Copper. The arrows indicate the spectral lines used for the temperature calculation.

The temporal detection window contained the laser pulse itself, but the laser's wavelength did not fall within the spectral detection range of the setup. The absence of continuum emission from Bremsstrahlung and radiative recombination processes, as reported previously [18], can be explained by the low irradiance used to create the plasma. As a result, a significant advantage of this configuration is that the use of a gated camera would not be necessary to trigger the detection window in order to avoid the continuum emission or the scattered laser light. However, the short lifetime of the plasma (300 ns), resulting from the low intensity of the laser and the small volume ablated from the sample, leads to a low duty cycle (300 ns/50 μs = 0.6%) in the case of non-triggered detection.

In order to determine the plasma excitation temperatures for Cu I and Cu II we analyzed several specific spectral transitions indicated by the arrows in Fig. 2 and listed in Table 1. No self-absorption was observed from the lineshape of the emission lines, allowing the use of resonant transitions in the temperature calculation. The excitation temperature was evaluated by the Boltzmann plot method using a Labview 8.5 program written specifically for our application. Each line listed in Table 1 is a single transition that was corrected for linear background and fitted with a Lorentzian profile:

#123146 - $15.00 USD Received 21 Jan 2010; revised 27 Mar 2010; accepted 29 Mar 2010; published 31 Mar 2010
(C) 2010 OSA

$$I(\lambda) = \frac{A}{\pi} \frac{\gamma}{(\lambda - \lambda_0)^2 + \gamma^2} + I_{bg} \quad (1)$$

where A is the integral of the peak, γ the half width at half maximum, λ_0 the central wavelength of the transition and I_{bg} the background intensity.

Table 1. List of lines in the calculation of the plasma temperature (λ: transition wavelength, gA: transition probability, E_{up}: upper level energy, E_{low}: lower level energy)

Cu I			Cu II		
λ (nm)	gA (10^8 s^{-1})[a]	E_{low}-E_{up} (eV)[b]	λ (nm)	gA (10^8 s^{-1})[c]	E_{low}-E_{up} (eV)[b]
261.84	1.23	1.389-6.123	202.55	4.2	2.975-8.864
282.44	0.47	1.389-5.777	204.38	13.44	2.719-8.917
324.75	5.56	0-3.817	205.5	8.6	2.833-9.095
327.4	2.74	0-3.786	211.21	12.27	3.256-9.125
458.7	1.92	5.102-7.805	214.9	4.48	2.719-8.486
465.11	3.04	5.072-7.737	217.94	11.85	2.975-8.663
510.55	0.08	1.389-3.817	227.63	1.62	2.975-8.421
			248.58	1.59	8.663-13.649
			250.63	1.73	8.486-13.482
			254.48	1.93	8.522-13.392

[a] From [19], [b] From [20], [c] From [21]

By inversion of the intensity I_{ij} of a spectral line, defined as:

$$I_{ij} = C \frac{hc}{\lambda_{ij}} g_j A_{ij} \frac{N_{I,II}}{Z_{I,II}(T_{I,II})} e^{-\frac{E_j}{T_{I,II}}}, \quad (2)$$

(where C is a constant taking into account the efficiency of the detection system, λ_{ij} and A_{ij} the wavelength and probability of the transition j→i, g_j and E_j the degeneracy and energy of the upper level j, $N_{I,II}$ the density, $T_{I,II}$ the excitation temperature and $Z_{I,II}$ the partition function of respectively Cu I and Cu II), the ratio $-\ln\left(\lambda_{ij} I_{ij} / g_j A_{ij}\right)$ was plotted as a function of E_j for each transition and fitted with a linear relation ($y = mx + p$) to obtain the corresponding excitation temperature from the inverse of the slope as shown in Eq. (3):

$$-\ln\left(\frac{\lambda_{ij} I_{ij}}{g_j A_{ij}}\right) = \frac{E_j}{T_{I,II}} + \ln\left(\frac{Z_{I,II}(T_{I,II})}{hcN_{I,II}}\right) \quad (3)$$

The obtained Boltzmann plots for Cu I and Cu II are shown in Fig. 3. This method gave a temperature for the neutral copper $T_{Cu\ I}$ = 2.61 ± 0.55 eV(30300 ± 6400 K) and for the singly ionized copper $T_{Cu\ II}$ = 2.68 ± 0.31 eV (31100 ± 3600 K). The degree of ionization α_{Cu} was evaluated by combination of the intercepts p_I and p_{II} of the respective Boltzmann plots for Cu I and Cu II (cf Eq. (3) as follows:

$$\begin{cases} N_I = \dfrac{Z_I(T_I)}{hcC} e^{-p_I} \\ N_{II} = \dfrac{Z_{II}(T_{II})}{hcC} e^{-p_{II}} \end{cases} \Rightarrow \alpha_{Cu} = \frac{N_{II}}{N_I + N_{II}} = \frac{1}{1 + \dfrac{Z_I(T_I) e^{-p_I}}{Z_{II}(T_{II}) e^{-p_{II}}}} \quad (4)$$

#123146 - $15.00 USD Received 21 Jan 2010; revised 27 Mar 2010; accepted 29 Mar 2010; published 31 Mar 2010
(C) 2010 OSA

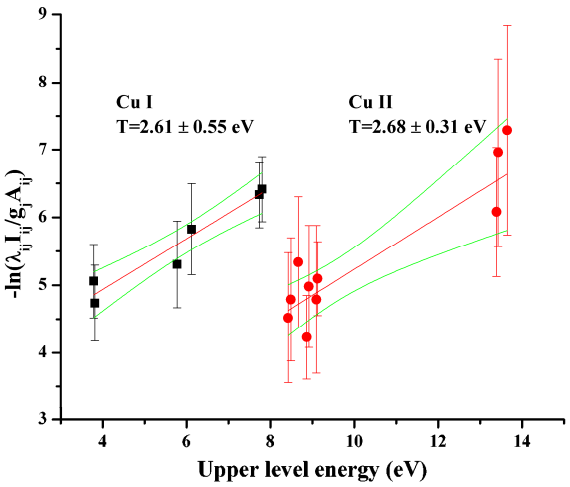

Fig. 3. Boltzmann plots for the calculation of the excitation temperature of Cu I and Cu II. Scatter symbols: experimental data, red curve: linear fit, green curve: prediction bands at 95%.

The degree of ionization was estimated at 61% leading to an electron density N_e of approximately $7 \cdot 10^{20}$ cm^{-3} evaluated from the Saha equation. This method of evaluation and the value it yields is subject to the propagation of measurement errors. Because the value obtained for N_e is 2 orders of magnitude less than the density of solid copper ($8 \cdot 10^{22}$ cm-3) and the plasma having a dimension on the order of hundreds of µm, this result is comparable to that published by Rieger *et al.* [18]. The minimum electron density for Local Thermodynamic Equilibrium (LTE), expressed as the McWhirter criterion, is thus $1.5 \cdot 10^{16}$ cm^{-3}, that is exceeded in the present plasma. Furthermore, the transient and inhomogeneous character of the plasma was taken into account, as mentioned by Cristoforetti *et al.* [22], in order to establish the validity of the LTE in the plasma.

The absence of emission lines from atmospheric nitrogen and oxygen atomic transitions is also an interesting result. Typical LIBS experiments show spectral lines around 744 nm and 777 nm respectively for the N I and the O I transitions for plasmas created at similar fluences under normal atmosphere [23]. In our case, perhaps the short lifetime of the plasma and the short detection gate didn't allow these transitions to appear in the spectrum.

4. Conclusion

We have performed the first LIBS experiments that employ a thulium fiber laser as the ablation source of copper. The low irradiance provided by the laser on the target surface appears to generate a plasma in Local Thermodynamic Equilibrium, with a temperature of approximately 2.6 eV and electron density around 10^{21} cm^{-3}. The low irradiance focused on a micrometric spot (less than 100 µm diameter) shows advantages as (i) the lack of continuum emission and (ii) no emission from atmospheric excitation. With continuing improvement, the performance of pulsed fiber lasers is approaching the pulse energy and pulse duration of conventional solid-state lasers used for Laser-Induced Breakdown Spectroscopy. Tm:fiber has the potential to greatly accelerate this improvement and enable the development of a new generation of LIBS systems utilizing rugged, compact and efficient fiber laser systems producing 1-10 ns pulses with multi-milliJoule energy at high repetition rates (>10 kHz). The development of such laser systems would greatly increase deployment flexibility.

5. Acknowledgments

This work was supported by DoD JTO MRI Contract W911NF-05-1-0517, ARO MURI Contract W911NF-06-1-0446 and the State of Florida.

#123146 - $15.00 USD Received 21 Jan 2010; revised 27 Mar 2010; accepted 29 Mar 2010; published 31 Mar 2010
(C) 2010 OSA